HHS Public Access

Author manuscript

Ultrasound Med Biol. Author manuscript; available in PMC 2018 November 01.

Published in final edited form as:

Ultrasound Med Biol. 2017 November ; 43(11): 2725–2732. doi:10.1016/j.ultrasmedbio.2017.07.012.

Combining subharmonic and ultraharmonic modes for intravascular ultrasound imaging: A preliminary evaluation

Himanshu Shekhar[a,*], **Jeffrey S. Rowan**[a], and **Marvin M. Doyley**[a]

[a]Department of Electrical and Computer Engineering, University of Rochester, Rochester NY 14627, USA

Abstract

Contrast-enhanced intravascular ultrasound (CE-IVUS) imaging could provide clinicians a valuable tool to assess cardiovascular risk and guide the choice of therapeutic strategies. In this technical note, we evaluated the feasibility of combining subharmonic and ultraharmonic imaging to improve the performance of CE-IVUS. Vessel phantoms perfused with phospholipid-shelled ultrasound contrast agents were visualized using subharmonic, ultraharmonic, and combined CE-IVUS modes with commercial peripheral and coronary imaging catheters. Flow channels as small as 0.8 mm and 0.5 mm were imaged at 12 MHz and 30 MHz transmit frequencies, respectively. Subharmonic and ultraharmonic imaging modes achieved a contrast-to-tissue ratio (CTR) up to 18.1 ± 1.8 dB and 19.6 ± 1.9 dB at 12 MHz, and 8.8 ± 1.8 and 12.5 ± 1.1 dB at 30 MHz transmit frequencies, respectively. Combining these modes improved the CTR to 32.5 ± 3.0 dB and 25.0 ± 1.6 dB at 12 and 30 MHz transmit frequencies. These results underscore the potential of combined-mode CE-IVUS imaging. Furthermore, the demonstration of this approach with commercial catheters may serve as a first step towards the clinical translation of CE-IVUS.

Keywords

vasa vasorum; intravascular ultrasound; subharmonic imaging; ultraharmonic imaging; ultrasound contrast agents; nonlinear imaging

Introduction

Neovascularization has been related to the progression and disruption of atherosclerotic plaques (Barger et al., 1984; Gössl et al., 2007). Plaque *vasa vasorum* serve as a pathway for inflammatory cells (Ritman and Lerman, 2007; Rademakers et al., 2013), leading to intraplaque hemorrhages and subsequent plaque rupture (Falk et al., 1995; Ten Kate et al., 2010). Contrast-enhanced ultrasound imaging techniques that exploit the linear and nonlinear response of ultrasound contrast agents (UCA) have been reported for imaging the

*Corresponding Author: Himanshu Shekhar, Present address: Department of Internal Medicine, University of Cincinnati Room #3933, CVC, Cincinnati, OH, 45267-0586; himanshu.shekhar@uc.edu; Phone, +1-513-558-8990.

vasa vasorum (Granada and Feinstein, 2008; Feinstein, 2006; Magnoni et al., 2009). It is envisaged that contrast-enhanced ultrasound could be used clinically to assess cardiovascular risk (Ten Kate et al., 2010) and to guide therapeutic interventions (Hellings et al., 2008, 2010). In particular, contrast-enhanced intravascular ultrasound imaging (CE-IVUS) is under development for imaging the *vasa vasorum* in the coronary and peripheral arteries (Goertz et al., 2006b, 2007). This approach relies on the administration of microbubble ultrasound contrast agents (UCA) along with minimally invasive imaging to visualize vascular organs and the microcirculation. In addition to *vasa vasorum* imaging, CE-IVUS could also be useful for plaque delineation (Sridharan et al., 2013), parametric imaging (Eisenbrey et al., 2012), endo-leak assessment (Partovi et al., 2015), and molecular imaging (Hamilton et al., 2004). Linear CE-IVUS imaging (Cachard et al., 1997) typically offers limited sensitivity and specificity, and may be confounded by motion artifacts. Recently, linear imaging based on radial modulation was reported to improve contrast-to-tissue ratio (CTR) by 7 – 15 dB relative to standard B-mode IVUS imaging (Yu et al., 2014). However, nonlinear imaging modes may be well suited for CE-IVUS, as they produce up to 30 dB improvement in CTR over linear imaging (Goertz et al., 2006b, 2007).

Several nonlinear CE-IVUS techniques have been reported using *in vitro* (Goertz et al., 2006a; Ma et al., 2015) and *in vivo* flow models (Goertz et al., 2006b, 2007). Nonlinear CE-IVUS imaging is typically performed with the aid of multi-pulse techniques such as pulse inversion imaging (Frijlink et al., 2011). The specificity of second harmonic CE-IVUS imaging can be reduced by nonlinear propagation (Goertz et al., 2006a). Subharmonic and ultraharmonic imaging modes are robust to artifacts produced from nonlinear propagation, leading to substantial improvements in CTR relative to fundamental-mode imaging (Goertz et al., 2007; Maresca et al., 2013; Daeichin et al., 2015). Acoustic angiography IVUS is another promising technique that employs excitation at conventional diagnostic frequencies and displays the signal from UCA at high frequencies (> 20 MHz) to reduce the impact of nonlinear propagation (Ma et al., 2015; Martin et al., 2016). The excellent resolution of acoustic angiography is encouraging for visualizing the microcirculation. However, the main limitation of this approach is that it requires a specialized dual-frequency transducer that is not commercially available. Furthermore, this approach relies on bubble destruction, and is therefore performed at lower frame rates to achieve adequate imaging sensitivity.

Goertz and colleagues pioneered nonlinear contrast-enhanced imaging using Intravascular ultrasound (Goertz et al., 2007, 2006b). These investigators employed a dual-frequency IVUS catheter to image the *vasa vasorum* using subharmonic (Goertz et al., 2007) and second harmonic (Goertz et al., 2006b) modes, both *in vitro* and in an *in vivo* atherosclerotic rabbit model. More recently, extensive studies were reported by Maresca and coworkers *in vitro* and in an *in vivo* chicken embryo model (Maresca et al., 2013, 2014). These studies demonstrated that when the transducer bandwidth is limited, ultraharmonic IVUS imaging can outperform other nonlinear imaging techniques. These studies were performed using prototype transducers constructed with lead magnesium niobate-lead titanate (PMN-PT) crystals that offer enhanced bandwidth and sensitivity relative to currently available IVUS transducers (Zhou et al., 2007). Although the development of broadband/specialized IVUS transducers (Zhou et al., 2007; Ma et al., 2014) is necessary in the long-term, demonstrating CE-IVUS with “off the shelf” catheters could simplify the pathway to United States Food

and Drug Administration approval and Conformité Européene mark, and accelerate the clinical translation of this technique.

Our group has reported an approach based on subharmonic filtering with a commercially available catheter (Eisenbrey et al., 2012; Sridharan et al., 2013). However, the CTR of subharmonic images produced in these studies was comparable to fundamental imaging, likely due to the limited bandwidth of the transducer, and the lack of contrast agent-specific pulsing sequences. Recently, we demonstrated the feasibility of ultraharmonic IVUS imaging using commercially available catheters (Shekhar et al., 2016; Huntzicker et al., 2016) by implementing long duration chirp pulses to attain CTRs ranging from 11 – 18 dB. Although these results are encouraging, combining nonlinear imaging modes could improve the performance of CE-IVUS imaging substantially. In this technical note, we investigated the feasibility of performing combined subharmonic and ultraharmonic CE-IVUS imaging using a single transmission. Commercially available peripheral and coronary imaging catheters were used along with a prototype IVUS system (Shekhar et al., 2016), and vessel flow phantoms perfused with a phospholipid-encapsulated contrast agent were visualized. The performance of standalone subharmonic and ultraharmonic imaging was compared with combined-mode CE-IVUS imaging.

Materials and Methods

A prototype imaging system (Fig. 1(a)) based on the iLab ™ IVUS scanner (Boston Scientific/Scimed, Natick, MA) and equipped with single-element imaging catheters — either Atlantis PV (8.5 F, 15 MHz center frequency, clinical use: peripheral imaging) or Atlantis SR Pro (3.2 F, 40 MHz center frequency, clinical use: coronary imaging) was employed. The −3 dB (full-width-half-maximum) fractional bandwidth of these transducers were 25 %, and 49 % (Shekhar et al., 2016). The imaging catheter was connected to the motor drive via a breakout box (provided by Boston Scientific) to circumvent the transmit and receive circuitry of the iLab ™ IVUS system (Yu et al., 2014). Two arbitrary function generators (models 33210A and 81150A, Agilent, Santa Clara, CA, USA) were used to (a) gate the amplifier, and (b) generate the excitation pulse, respectively. The excitation frequencies were chosen considering the tradeoff between transducer sensitivity in the transmit and nonlinear receive modes (both subharmonic and ultraharmonic). Accordingly, the transducers with 15 MHz and 40 MHz center frequencies were used to transmit pulses at 12 MHz and 30 MHz, respectively. Specifically, the excitation pulse for 12 MHz and 30 MHz transmit consisted of linear frequency modulated chirps (10 % fractional bandwidth), with 1.67 μs and 0.67 μs pulse duration, respectively (Shekhar and Doyley, 2012; Shekhar et al., 2016). Excitation pulses were tapered using a 70 % Tukey window to reduce pulse distortion. A pulse repetition frequency of 10.8 kHz was used for imaging at both frequencies. The excitation pulses were boosted by 43 dB using a linear pulse amplifier (MR 5000 DA, ENI, Rochester, NY) and relayed to the IVUS transducer through a diplexer (RDX-6, Ritec Inc., Warwick, RI). For imaging at 30 MHz transmit frequency, a custom lowpass filter (E&I, Rochester, NY, USA) with −3 dB cutoff frequency of 34 MHz was used to filter the amplifier output to eliminate nonlinearity in the transmit signal. The IVUS transducers were calibrated as reported earlier (Shekhar et al., 2016). Peak pressures measured on axis with the peripheral and coronary imaging catheters at distances of 5 mm

and 2.5 mm were 2.3 and 1.4 MPa, respectively. The motor used to drive the IVUS transducer had a constant rotation speed of 30 revolutions/second which produced standard frame acquisition rates (30 frames/second).

The studies reported in this technical note were performed using phospholipid shelled UCA (Shekhar et al., 2016) that encapsulate decafluorobutane gas (Targestar-P® and Targestar-P-HF ®, Targeson Inc., San Diego, CA). Targestar-P®, which is recommended by the manufacturer for imaging at 1 to 15 MHz range, was used to perform imaging at 12 MHz. Targestar-P-HF® was used to perform imaging at 30 MHz, because it is indicated for imaging in the 15 – 40 MHz range. The size distribution of these agents has been reported previously (Shekhar et al., 2016), and the mean number-weighted diameter of Targestar-P® and Targestar-P-HF® are 1.7 μm and 1.1 μm, respectively (Shekhar et al., 2016). Vessel phantoms (Figure 1(b)) similar to those reported previously (Shekhar et al., 2016) were used. The phantom used for imaging at 12 MHz had a 7-mm main lumen and three side channels with 2.2, 1.6 and 0.8 mm diameters, located at a 5 mm radial distance from the center of the main lumen. The phantom used for 30-MHz imaging had a 3 mm diameter main lumen, and a single side channel of 0.5 mm diameter located at a radial distance of 2.5 mm from the center of the main lumen. A programmable syringe pump (Pump 11, Harvard Apparatus, Holliston, MA) was used to introduce contrast agent into the side channel(s) of the phantom at a flow rate of 9 mL/min. The main lumen of the artery was not perfused with UCA. This configuration can be achieved *in vivo* by clearing the lumen with a saline flush (Honye et al., 1999; Martin et al., 2016). Targestar-P® was diluted in deionized water to achieve concentrations of 2.1×10^6 microbubbles/ml for imaging using the peripheral imaging catheter and 1.05×10^7 microbubbles/ml for imaging with the coronary imaging catheter, consistent with our previous publication (Shekhar et al., 2016). The radio frequency (RF) echoes received from the flow phantom perfused with Targestar-P® were boosted by 60 dB using the receiving stage of a pulser-receiver (JSR 300, JSR, Waltham, MA, USA), and sampled at 12 bit amplitude resolution using a PCI bus data acquisition card (Acquiris DP 310, Agilent, Santa Clara, CA, USA). The sampling frequency used for 12 MHz and 30 MHz transmit cases were 200 MHz and 357 MHz, respectively. All analyses and signal processing were performed offline using MATLAB® (The Mathworks Inc., Natick, MA, USA).

To produce fundamental B-mode images, envelope detection and polar-to-Cartesian coordinate transformation was performed on the received echoes. To produce subharmonic images and ultraharmonic images, 12 th order zero-phase Butterworth filters (−3 dB corner frequencies shown in Table 1) were used before performing envelope-detection and coordinate transformation. Subharmonic and ultraharmonic imaging frames were averaged to produce the combined CE-IVUS images. All CE-IVUS images were processed to remove impulse noise (Shekhar et al., 2016). The contrast-to-tissue ratio (CTR) was used to evaluate the performance of imaging as described previously (Shekhar et al., 2016; Maresca et al., 2013, 2014; Yu et al., 2014; Goertz et al., 2006b). The regions of interest (ROI) used to compute the CTR were positioned at the same radial location from the catheter, to prevent CTR estimates from being confounded by any spatial variability in the echogenecity of the phantom (Shekhar et al., 2016).

Results

Figures 2 shows representative (a) fundamental, (b) subharmonic, (c) ultraharmonic, and (d) combined-mode CE-IVUS images acquired at 12 MHz transmit frequency with the peripheral imaging catheter. The flow channels were not visible in the fundamental CE-IVUS images, but were clearly visible in nonlinear CE-IVUS images. Some artifacts were observed at the boundary of the main lumen and the phantom because of saturation during data acquisition in all images. Figure 3 shows the (a) fundamental, (b) subharmonic and (c) ultraharmonic IVUS images generated using 30 MHz transmit frequency with the coronary imaging catheter. The 0.5-mm flow channel was visible in nonlinear CE-IVUS (between 9 ‘o’ clock and 11 ‘o’ clock). The background signal from the phantom signal was reduced in both subharmonic and ultraharmonic images, but not completely eliminated. In particular, a “spiral” artifact originating from electronic noise was observed in Figure 3(b). The spiral artifact was caused by the presence of an electronic noise peak in the RF signal. This noise peak was observed to traverse through the signal over depth in a periodic manner. Due to the time dependent nature of this peak, it was observed at different depths in the subsequent RF lines, which created the appearance of a spiral. Although this artifact was present in all images, it was below the display dynamic range, except in Figure 3(b). However, both the background signal and artifacts were suppressed below the noise floor for the combined CE-IVUS. The images shown in figures 2 and 3 demonstrate that combined-mode CE-IVUS improves the visualization of flow channels substantially relative to standalone implementation of subharmonic and ultraharmonic imaging. Table 2 reports the CTR attained with subharmonic, ultraharmonic and combined-mode imaging at 12 MHz, and 30 MHz transmit frequencies. The performance of subharmonic and ultraharmonic modes was comparable. The CTR obtained by combining subharmonic and ultraharmonic modes was substantially higher than that obtained using these modes separately.

Discussion

This study is the first demonstration of combined subharmonic and ultraharmonic IVUS imaging, which was realized with commercial bandlimited IVUS catheters. The envelope of the ultraharmonic and subharmonic signal from UCA adds up constructively, leading to an enhancement in the signal from the contrast infused region. However, the noise in the subharmonic and ultraharmonic band is uncorrelated and can be reduced by averaging frames. The combined effect of increase in UCA signal and a reduction in noise is an improved contrast-to-tissue ratio. Nonlinear imaging modes such as subharmonic and ultraharmonic imaging typically employ narrowband pulsing. However, adequate sensitivity at both the transmit and the receive frequency is required, which has made it challenging until recently to achieve these modes using commercial catheters with limited bandwidth. Furthermore, combined subharmonic and ultraharmonic imaging mode presents even more stringent bandwidth requirements, given that the transducer is expected to be adequately sensitive at the transmit frequency, as well as both subharmonic and ultraharmonic frequency bands. Although the subharmonic and ultraharmonic frequencies were outside the FWHM bandwidth of the transducers used in this study, the usable bandwidth depends on the signal-to-noise ratio, and can be higher than the FWHM bandwidth. The subharmonics and ultraharmonic response of UCA has been reported to increase sharply with pressure

(Daeichin et al., 2015), and grows over the duration of the transmit cycles (Cheung et al., 2008). In this study, used custom amplification to generate adequate transmit pressures, and long duration chirp pulses to obtain a strong nonlinear response from UCA (Zhang et al., 2007; Shekhar and Doyley, 2013; Harput et al., 2013) which enabled us to overcome bandwidth limitations of the IVUS transducers. The main limitation of imaging with long-duration pulses is that the axial resolution is reduced. However, lower thresholds are observed for subharmonic and ultraharmonic emissions, and the spectral leakage of the fundamental frequency into the nonlinear frequency bands is minimal (Shekhar et al., 2016). We employed chirp pulses to realize long duration pulsing because they have been previously reported to improve nonlinear signal from UCA over sine-burst pulses of the same duration and center frequency (Maresca et al., 2014; Shekhar and Doyley, 2012, 2013; Harput et al., 2013). Butterworth filtering was used to isolate subharmonic and ultraharmonic modes. The background signal from the tissue mimicking phantom was suppressed adequately by filtering, without the need for multi-pulse techniques such as pulse inversion which reduce frame rate and could introduce motion artifacts. Matched filtering can also be used to isolate subharmonic and ultraharmonic signals (Shekhar et al., 2016). However, when matched filtering was used to isolate subharmonic and ultraharmonic modes, up to 5 dB lower CTR was achieved in each case (data not shown), likely because of spectrally overlapped frequency bands, which cause side lobes that may degrade image contrast (Harput et al., 2014).

Phospholipid-shelled bubbles have been shown to produce nonlinear emissions at lower pressures than polymer and albumin-encapsulated microbubbles, therefore they are well suited for nonlinear IVUS imaging. Although two different sizes of UCA were used for this study for imaging at transmit frequencies of 12 MHz and 30 MHz, the UCA sizes were not necessarily optimized for subharmonic and ultraharmonic imaging at these frequencies. If the size distribution of the agent is modified suitably, the nonlinear signal could be improved further (Shekhar et al., 2013). Targestar-P® is presently available only for preclinical research. However, we anticipate that the results of this study could be reproduced with clinically available UCA such as Definity® (Lantheus Medical Imaging, North Billerica, MA), because extensive work has been reported previously for subharmonic and ultraharmonic IVUS imaging with native and size-isolated populations of Definity® (Goertz et al., 2007; Maresca et al., 2013) for the range of pressures achievable with the current system.

The experiments reported in this technical note were performed in a simplified in vitro setting. Nonetheless, these experiments represent the first step towards developing a CE-IVUS system for vasa vasorum imaging and other vascular imaging applications. Nonlinear CE-IVUS imaging studies typically report reduced frame rates, either to allow the replenishment of destroyed microbubbles (Ma et al., 2015) or to improve the SNR by averaging (Goertz et al., 2007; Maresca et al., 2013). The images reported in this study were acquired at standard frame rates (30 frames/second), which is encouraging for the clinical adoption of subharmonic IVUS imaging. The CTR achieved in this study with standalone subharmonic and ultraharmonic imaging modes was comparable to that reported with chirp reversal (Maresca et al., 2012), radial modulation (Yu et al., 2014) and acoustic angiography (Ma et al., 2015) imaging. Notably, the CTRs achieved with combined subharmonic and

ultraharmonic imaging were higher than that achieved in these previously reported studies and approached the CTR of subharmonic imaging reported with a prototype dual-frequency catheter (Goertz et al., 2007). However, it is important to consider that the *in vivo* studies by Goertz et al. (2007) used lower pressures and shorter excitation pulses, which could reduce UCA disruption and improve the axial resolution of imaging. Furthermore, these investigators performed *in vivo* imaging without clearing the contrast agent from the main lumen. Flushing the main lumen to clear UCA will also clear the contrast in the *vasa vasorum* after some delay, reducing the total number of frames that can be acquired. Presence of UCA in the main lumen may also contribute to nonlinear propagation (Tang and Eckersley, 2006; ten Kate et al. 2012). However, subharmonic and ultraharmonic imaging modes are considered to be relatively robust to the artifacts caused by nonlinear propagation (Daeichin et al., 2015).

The results reported in this technical note must be interpreted carefully given its limitations. First, the use of long duration imaging can result in ring down artifacts, which may make the interpretation of structures located very close (< 1 mm distance) to the catheter. Second, the attenuation coefficient of the phantom used in this preliminary study (0.2 dB/cm/MHz) was lower than arterial tissue (0.5 dB/cm/MHz), which is a major limitation of this study. However, given the limited distance traversed by ultrasound through the phantom (1-way distance of 1.5 mm and 1 mm for 12 MHz and 30 MHz, respectively), the additional (one-way) attenuation incurred for the transmit beam would only be 0.54 dB at 12 MHz and 0.9 dB at 30 MHz transmit frequencies,. Therefore, we do not anticipate a major change in the imaging performance observed in this study because of this limitation. Nonetheless, we plan to perform studies in future using an *in vivo* model to assess the imaging performance under more realistic conditions. Third, while the images reported in this study were acquired at real time frame rates, they were processed offline. Future work will focus on developing real time image visualization software. Fourth, this study employed higher transmit pressures and pulse durations than those reported previously (Goertz et al., 2007; Maresca et al., 2013, 2014), to improve CTR for imaging with limited bandwidth IVUS catheters. However, using higher pressures can accelerate UCA disruption and only few image frames can be acquired before the loss of contrast from UCA. Lastly, the diameters of the flow channels used in this preliminary study were larger than the microcirculation. For example, detection of a single large channel is likely less challenging than detecting a network of *vasa vasorum* in the *in vivo* setting. This is because the *vasa vasorum* will likely appear as a more diffuse structure than a single vessel with a clearly delineated boundary. We are currently in the process of developing a vessel phantom that models the *vasa vasorum* and the lumen more realistically. We plan to conduct more extensive *in vitro* studies with this vessel phantom along with *in vivo* studies to demonstrate the feasibility of *vasa vasorum* imaging using combined subharmonic and ultraharmonic imaging.

Conclusions

This study demonstrates that combined subharmonic and ultraharmonic imaging improves imaging performance relative to the standalone implementation of these modes. Furthermore, combined ultraharmonic and subharmonic imaging mode was feasible using commercially available bandlimited IVUS catheters. Contrast-to-tissue ratios of up to 25

± 1.6 dB and 33 ± 3 dB were achieved using combined CE-IVUS mode for 12 MHz and 30 MHz transmit frequencies, respectively. Additionally, these results were obtained at real time acquisition rates, which supports the continued investigation of combined CE-IVUS for preclinical research and clinical imaging.

Acknowledgments

This work was funded by the National Heart Lung and Blood Institute (R01 HL088523). Himanshu Shekhar was supported in part by the Howard Hughes Medical Institute Med-to-Grad Fellowship. The authors thank Ivy Awuor, Steven Huntzicker, and Targeson Inc. for technical assistance.

References

Barger AC, Beeuwkes R III, Lainey LL, Silverman KJ. Hypothesis: vasa vasorum and neovascularization of human coronary arteries. a possible role in the pathophysiology of atherosclerosis. The New England journal of medicine. 1984; 310:175–177. [PubMed: 6197652]

Cachard C, Finet G, Bouakaz A, Tabib A, Françon D, Gimenez G. Ultrasound contrast agent in intravascular echography: an in vitro study. Ultrasound Med Biol. 1997; 23:705–717. [PubMed: 9253818]

Cheung K, Couture O, Bevan P, Cherin E, Williams R, Burns P, Foster F. In vitro characterization of the subharmonic ultrasound signal from definity microbubbles at high frequencies. Physics in medicine and biology. 2008; 53:1209. [PubMed: 18296758]

Daeichin V, Bosch JG, Needles A, Foster FS, van der Steen A, de Jong N. Subharmonic, non-linear fundamental and ultraharmonic imaging of microbubble contrast at high frequencies. Ultrasound in medicine & biology. 2015; 41:486–497. [PubMed: 25592458]

Eisenbrey JR, Sridharan A, deMuinck ED, Doyley MM, Forsberg F. Parametric subharmonic imaging using a commercial intravascular ultrasound scanner an in vivo feasibility study. J Ultrasound Med. 2012; 31:361–371. [PubMed: 22368126]

Falk E, Shah PK, Fuster V. Coronary plaque disruption. Circulation. 1995; 92:657–71. [PubMed: 7634481]

Feinstein S. Contrast ultrasound imaging of the carotid artery vasa vasorum and atherosclerotic plaque neovascularization. Journal of the American College of Cardiology. 2006; 48:236–243. [PubMed: 16843169]

Frijlink, ME., Goertz, DE., Van Der Steen, AFW. Pulse inversion sequences for nonlinear imaging. US Patent. 7,967,753. 2011.

ten Kate GL, Renaud GG, Akkus Z, van den Oord SC, ten Cate FJ, Shamdasani V, Entrekin RR, Sijbrands EJ, de Jong N, Bosch JG, Schinkel AF, van der Steen AF, et al. Far-wall pseudoenhancement during contrast-enhanced ultrasound of the carotid arteries: clinical description and in vitro reproduction. Ultrasound Med Biol. 2012; 38:593–600. [PubMed: 22341054]

Goertz D, Frijlink M, De Jong N, Van Der Steen A. Nonlinear intravascular ultrasound contrast imaging. Ultrasound Med Biol. 2006a; 32:491–502. [PubMed: 16616596]

Goertz DE, Frijlink ME, Tempel D, Bhagwandas V, Gisolf A, Krams R, de Jong N, van der Steen AF. Subharmonic contrast intravascular ultrasound for vasa vasorum imaging. Ultrasound Med Biol. 2007; 33:1859–72. [PubMed: 17683850]

Goertz DE, Frijlink ME, Tempel D, van Damme LC, Krams R, Schaar JA, Ten Cate FJ, Serruys PW, de Jong N, van der Steen AF. Contrast harmonic intravascular ultrasound: a feasibility study for vasa vasorum imaging. Invest Radiol. 2006b; 41:631–8. [PubMed: 16829746]

Gössl M, Versari D, Mannheim D, Ritman EL, Lerman LO, Lerman A. Increased spatial vasa vasorum density in the proximal lad in hypercholesterolemia implications for vulnerable plaque-development. Atherosclerosis. 2007; 192:246–252. [PubMed: 16919638]

Granada J, Feinstein S. Imaging of the vasa vasorum. Nature Clinical Practice Cardiovascular Medicine. 2008; 5:S18–S25.

Hamilton AJ, Huang SL, Warnick D, Rabbat M, Kane B, Nagaraj A, Klegerman M, McPherson DD. Intravascular ultrasound molecular imaging of atheroma components in vivo. J Am Coll Cardiol. 2004; 43:453–460. [PubMed: 15013130]

Harput S, Arif M, McLaughlan J, Cowell DJ, Freear S. The effect of amplitude modulation on subharmonic imaging with chirp excitation. IEEE Trans Ultrason, Ferroelect, Freq Control. 2013; 60:2532–2544.

Harput S, McLaughlan J, Cowell DM, Freear S. Superharmonic imaging with chirp coded excitation: Filtering spectrally overlapped harmonics. IEEE Trans Ultrason, Ferroelect, Freq Control. 2014; 61:1802–1814.

Hellings WE, Moll FL, De Vries JPP, Ackerstaff RG, Seldenrijk KA, Met R, Velema E, Derksen WJ, De Kleijn DP, Pasterkamp G. Atherosclerotic plaque composition and occurrence of restenosis after carotid endarterectomy. Jama. 2008; 299:547–554. [PubMed: 18252885]

Hellings WE, Peeters W, Moll FL, Piers SR, van Setten J, Van der Spek PJ, de Vries JPP, Seldenrijk KA, De Bruin PC, Vink A, et al. Composition of carotid atherosclerotic plaque is associated with cardiovascular outcome a prognostic study. Circulation. 2010; 121:1941–1950. [PubMed: 20404256]

Honye J, Saito S, Takayama T, Yajima J, Shimizu T, Chiku M, Mizumura T, Takaiwa Y, Horiuchi K, Moriuchi M, et al. Clinical utility of negative contrast intravascular ultrasound to evaluate plaque morphology before and after coronary interventions. The American journal of cardiology. 1999; 83:687–690. [PubMed: 10080419]

Huntzicker S, Shekhar H, Doyley MM. Contrast-enhanced quantitative intravascular elastography: The impact of microvasculature on model-based elastography. Ultrasound in medicine & biology. 2016; 42:1167–1181. [PubMed: 26924697]

Ma J, Martin K, Dayton P, Jiang X. A preliminary engineering design of intravascular dual-frequency transducers for contrast-enhanced acoustic angiography and molecular imaging. Ultrasonics, Ferroelectrics and Frequency Control, IEEE Transactions on. 2014; 61:870–880.

Ma J, Martin KH, Li Y, Dayton PA, Shung KK, Zhou Q, Jiang X. Design factors of intravascular dual frequency transducers for super-harmonic contrast imaging and acoustic angiography. Phys Med Biol. 2015; 60:3441. [PubMed: 25856384]

Magnoni M, Coli S, Marrocco-Trischitta M, Melisurgo G, De Dominicis D, Cianflone D, Chiesa R, Feinstein S, Maseri A. Contrast-enhanced ultrasound imaging of periadventitial vasa vasorum in human carotid arteries. European Journal of Echocardiography. 2009; 10:260–264. [PubMed: 18757860]

Maresca D, Jansen K, Renaud G, Van Soest G, Li X, Zhou Q, De Jong N, Shung K, Van der Steen A. Intravascular ultrasound chirp imaging. Appl Phy Lett. 2012; 100:043703-1–043703-3.

Maresca D, Renaud G, van Soest G, Li X, Zhou Q, Shung KK, de Jong N, van der Steen AF. Contrast-enhanced intravascular ultrasound pulse sequences for bandwidth-limited transducers. Ultrasound Med Biol. 2013; 39:706–13. [PubMed: 23384459]

Maresca D, Skachkov I, Renaud G, Jansen K, Van Soest G, De Jong N, Van der Steen A. Imaging microvasculature with contrast-enhanced ultraharmonic ultrasound. Ultrasound Med Biol. 2014; 40:1318–1328. [PubMed: 24613639]

Martin KH, Lindsey BD, Ma J, Nichols TC, Jiang X, Dayton PA. Ex vivo porcine arterial and chorioallantoic membrane acoustic angiography using dual-frequency intravascular ultrasound probes. Ultrasound Med Biol. 2016; 42:2294–307. [PubMed: 27260246]

Partovi S, Kaspar M, Aschwanden M, Lopresti C, Madan S, Uthoff H, Imfeld S, Staub D. Contrast-enhanced ultrasound after endovascular aortic repair: current status and future perspectives. Cardiovasc Diagn Ther. 2015; 5:454–463. [PubMed: 26673398]

Rademakers T, Douma K, Hackeng TM, Post MJ, Sluimer JC, Daemen MJ, Biessen EA, Heeneman S, van Zandvoort MA. Plaque-associated vasa vasorum in aged apolipoprotein e–deficient mice exhibit proatherogenic functional features in vivo. Arteriosclerosis, thrombosis, and vascular biology. 2013; 33:249–256.

Ritman E, Lerman A. The dynamic vasa vasorum. Cardiovascular research. 2007; 75:649–658. [PubMed: 17631284]

Shekhar H, Doyley M. The response of phospholipid-encapsulated microbubbles to chirp-coded excitation: Implications for high-frequency nonlinear imaging. J Acoust Soc Am. 2013; 133:3145. [PubMed: 23654417]

Shekhar H, Doyley MM. Improving the sensitivity of high-frequency subharmonic imaging with coded excitation: A feasibility study. Med Phys. 2012; 39:2049–60. [PubMed: 22482626]

Shekhar H, Huntzicker S, Awuor I, Doyley MM. Chirp-coded ultraharmonic imaging with a modified clinical intravascular ultrasound system. Ultrason Imaging. 2016; 38:403–419. [PubMed: 26634777]

Shekhar H, Rychak JJ, Doyley MM. Modifying the size distribution of microbubble contrast agents for high-frequency subharmonic imaging. Med Phys. 2013; 40:082903-1–10. [PubMed: 23927358]

Sridharan A, Eisenbrey JR, Machado P, Doyley MM, Forsberg F. Delineation of atherosclerotic plaque using subharmonic imaging filtering techniques and a commercial intravascular ultrasound system. Ultrason Imaging. 2013; 35:30–44. [PubMed: 23287505]

Tang MX, Eckersley RJ. Nonlinear propagation of ultrasound through microbubble contrast agents and implications for imaging. IEEE transactions on ultrasonics, ferroelectrics, and frequency control. 2006; 53

Ten Kate GL, Sijbrands EJ, Valkema R, ten Cate FJ, Feinstein SB, Van der Steen AF, Daemen MJ, Schinkel AF. Molecular imaging of inflammation and intraplaque vasa vasorum: A step forward to identification of vulnerable plaques? Journal of Nuclear Cardiology. 2010; 17:897–912. [PubMed: 20552308]

Yu F, Villanueva F, Chen X. Radial modulation contrast imaging using a 20-mhz single-element intravascular ultrasound catheter. IEEE Trans Ultrason, Ferroelect, Freq Control. 2014; 61:779–791.

Zhang D, Gong Y, Gong X, Liu Z, Tan K, Zheng H. Enhancement of subharmonic emission from encapsulated microbubbles by using a chirp excitation technique. Physics in medicine and biology. 2007; 52:5531–44. [PubMed: 17804880]

Zhou Q, Xu X, Gottlieb EJ, Sun L, Cannata JM, Ameri H, Humayun MS, Han P, Shung KK. Pmn-pt single crystal, high-frequency ultrasonic needle transducers for pulsed-wave doppler application. Ultrasonics, Ferroelectrics and Frequency Control, IEEE Transactions on. 2007; 54:668–675.

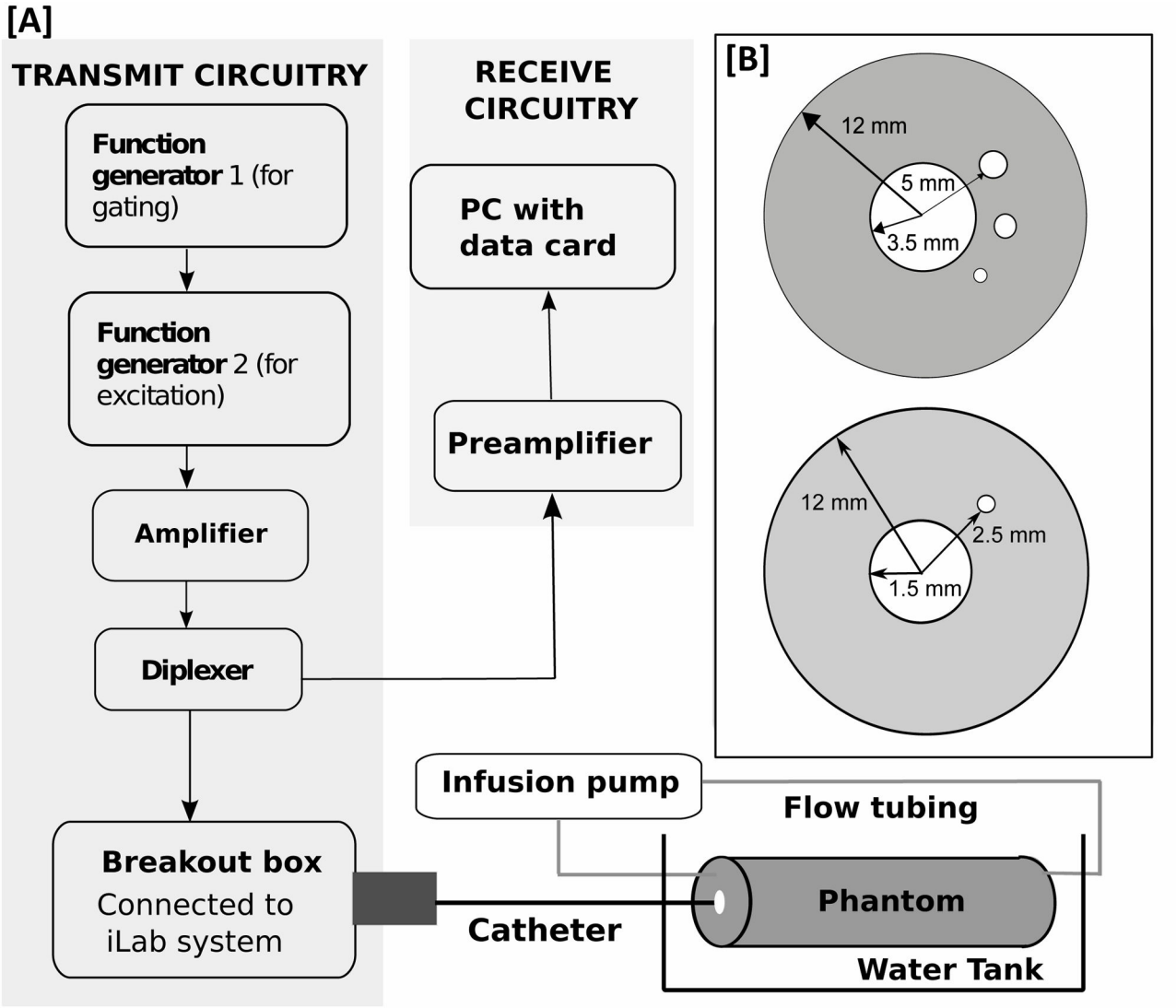

Figure 1.
(a) A schematic of the system and (b) the phantoms employed for CE-IVUS imaging.

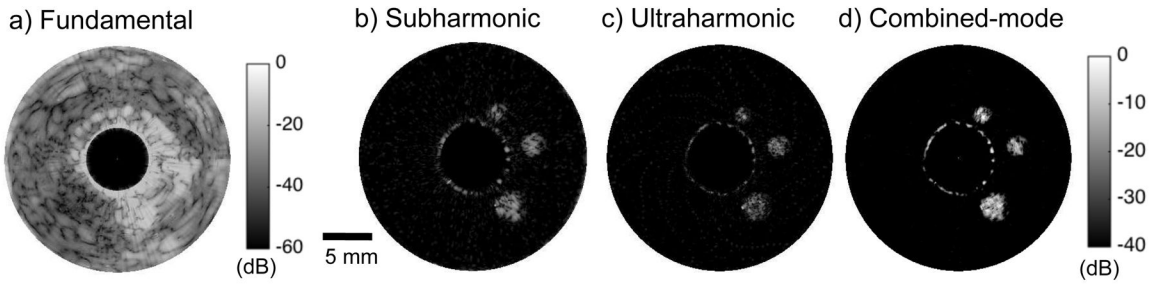

Figure 2.

The (a) fundamental, (b) subharmonic, (c) ultraharmonic, and (d) combined-mode CE-IVUS images acquired at 12 MHz transmit frequency. The fundamental and nonlinear CE-IVUS images are displayed at dynamic ranges of 60 dB and 40 dB, respectively to aid visualization. The combined imaging mode achieved higher contrast-to-tissue ratio than standalone use of subharmonic and ultraharmonic imaging modes.

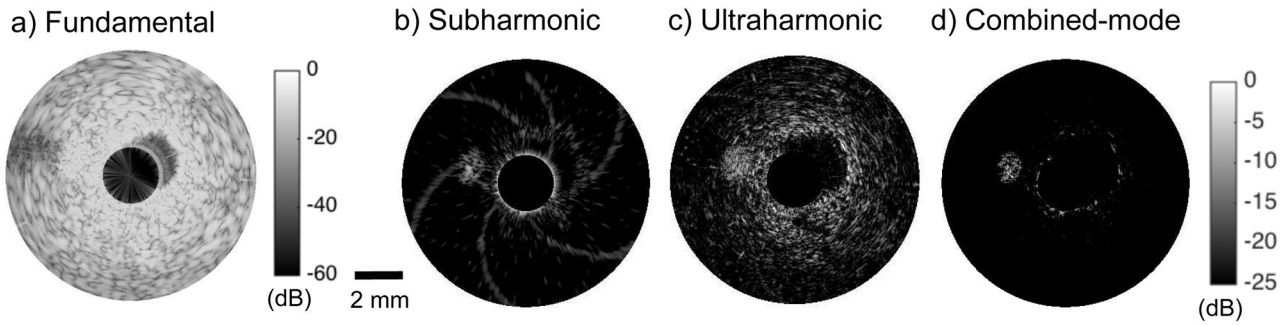

Figure 3.

The (a) fundamental, (b) subharmonic, (c) ultraharmonic, and (d) combined-mode CE-IVUS images acquired at 30 MHz transmit frequency. The fundamental and nonlinear CE-IVUS images are displayed at dynamic ranges of 60 dB and 25 dB, respectively to aid visualization. The combined imaging mode improved imaging performance relative to subharmonic and ultraharmonic imaging.

Table 1

The −3 dB corner frequencies used for Butterworth filtering to display subharmonic and ultraharmonic CE-IVUS imaging modes.

Transmit frequency	*Subharmonic*	*Ultraharmonic*
12 MHz	(5 MHz, 7 MHz)	(17 MHz, 19 MHz)
30 MHz	(14 MHz, 16 MHz)	(44 MHz, 46 MHz)

Table 2

The contrast-to-tissue ratio (CTR) obtained with subharmonic, ultraharmonic and combined-mode CE-IVUS.

Transmit frequency	*Subharmonic*	*Ultraharmonic*	*Combined*
12 MHz	18.1± 1.8 dB	19.6± 1.9 dB	32.5± 3.0 dB
30 MHz	8.8± 1.8 dB	12.5± 1.1 dB	25.0± 1.6 dB